Sheps, L., Rotavera, B., Eskola, A., Osborn, D., Taatjes, C., Au, K., Shallcross, D., Khan, A., & Percival, C. (2017). The reaction of Criegee intermediate CH_2OO with water dimer: primary products and atmospheric impact. *Physical Chemistry Chemical Physics*, *19*(33), 21970-21979. https://doi.org/10.1039/C7CP03265J

The Reaction of Criegee Intermediate CH_2OO with Water Dimer: Primary Products and Atmospheric Impact

Leonid Sheps,[a,*] Brandon Rotavera,[a,§] Arkke J. Eskola,[a,†] David L. Osborn,[a] Craig A. Taatjes,[a] Kendrew Au,[a] Dudley E. Shallcross,[b] M. Anwar H. Khan,[b] and Carl J. Percival[c,‡]

[a.] Combustion Research Facility, Sandia National Laboratories, 7011 East Ave., MS 9055, Livermore, California 94551 USA. Email: lsheps@sandia.gov

[b.] Biogeochemistry Research Centre, School of Chemistry, University of Bristol, Cantock's Close BS8 1TS, UK.

[c.] The Centre for Atmospheric Science, School of Earth, Atmospheric and Environmental Science, University of Manchester, Simon Building, Brunswick Street, Manchester, M13 9PL, UK.

§ Present address: College of Engineering, University of Georgia, 597 DW Brooks Dr., Athens, GA 30602 USA; Department of Chemistry, University of Georgia, 140 Cedar St., Athens, GA 30602 USA

† Present address: Department of Chemistry, University of Helsinki, A. I. Virtasen aukio 1, Helsinki, Finland

‡ Present address: Jet Propulsion Laboratory, 4800 Oak Grove Dr., Pasadena, CA 91109 USA

Electronic Supplementary Information (ESI) available: Details of experimental data analysis and global atmospheric model

* email: lsheps@sandia.gov

Abstract

The rapid reaction of the smallest Criegee intermediate, CH_2OO, with water dimers is the dominant removal mechanism for CH_2OO in the Earth's atmosphere, but its products are not well understood. This reaction was recently suggested as a significant source of the most abundant tropospheric organic acid, formic acid (HCOOH), which is consistently underpredicted by atmospheric models. However, using time-resolved measurements of reaction kinetics by UV absorption and product analysis by photoionization mass spectrometry, we show that the primary products of this reaction are formaldehyde and hydroxymethyl hydroperoxide (HMHP), with direct HCOOH yields of less than 10%. Incorporating our results into a global chemistry-transport model further reduces HCOOH levels by 10 – 90%, relative to previous assumptions, which indicates that the reaction CH_2OO + water dimer by itself cannot resolve the discrepancy between the measured and predicted HCOOH levels.

Introduction

Criegee intermediates (CI) are carbonyl oxides, formed by ozonolysis of alkenes[1,2] and long recognized as key players in the Earth's troposphere through chemically activated decomposition (a dominant non-photolytic source of OH) and bimolecular reactions with trace atmospheric species.[3] Until recently our knowledge of gas-phase CI reactivity came either from indirect experiments using complex reaction analysis or from computational work.[4,5] As a consequence, the atmospheric impact of CI reactions was subject to large uncertainties. However, a recent discovery by Taatjes and co-workers of an efficient alternative route[6,7] to form large quantities of stabilized CI in the lab has opened the door to direct spectroscopic and kinetic studies. The electronic structure and photochemistry of CI are increasingly well characterized by experimental studies[8] and high-level quantum chemical calculations.[9,10] Meanwhile, direct kinetics measurements have led to a reassessment[3] of the role of CI in the oxidizing capacity of the atmosphere and in tropospheric budgets of organic acids, secondary organic aerosols, ozone, NO_x, NO_y and HO_x.[11-14]

Because Criegee intermediates form during ozonolysis of abundant hydrocarbons such as isoprene, accurate knowledge of product branching in their reactions is important for the understanding of atmospheric oxidative pathways. The simplest CI, CH_2OO, was found to react much more rapidly with SO_2, NO_2, and carboxylic acids than previously assumed.[6,7,15,16] However, the full impact of its reactivity on the atmosphere depends on the competition among CH_2OO reactions with trace species and with water vapor. Recent theory[17,18] and laboratory[19-22] studies show that although the reaction $CH_2OO + H_2O$ is relatively slow, the reaction with water dimer, $(H_2O)_2$, is fast enough to act as the primary removal route of CH_2OO under most conditions in the atmosphere.

The consensus, based on prior experiments,[23-25] theory,[17,18] and modeling,[26-29] was that the reaction of CH_2OO with water monomer or dimer forms mainly hydroxymethyl hydroperoxide (HMHP), which further reacts to produce formic acid (HCOOH),[30] H_2O_2, and formaldehyde (CH_2O).[25,31,32] However, a more recent extensive study by Wennberg and co-workers[33] concluded that the reaction $CH_2OO + (H_2O)_2$ directly produces formic acid with a yield of 54%. A 2015 review by Millet *et al.*[34] showed that formic acid is consistently underpredicted by current models and suggested a large unidentified HCOOH source. The authors considered several possible "missing" sources of HCOOH, including direct biogenic emission, heterogeneous conversion, or reactive formation from multiple sources. The model by Millet *et al.*[34] assumed fast conversion of either CH_2OO or HMHP to HCOOH; however, definitive assessment of the role of CH_2OO chemistry as a source of HCOOH requires a reliable quantification of the products of its reaction with water.

Previous experimental measurements of the products in the reaction of CH_2OO with water vapor relied on time-averaged detection of species in quasi-steady state reactors. The derivation of product yields in such studies can be vulnerable to uncertainties in chemical mechanisms, and identification of primary products may be challenging. Here we report direct time-resolved measurements of the reaction of CH_2OO with water, showing far smaller primary yields of formic acid than suggested by Nguyen *et al*.[33] Our results limit the possible direct contribution of CH_2OO to tropospheric HCOOH and highlight the need to explore the subsequent chemistry of CI reaction products for accurate modeling of organic acid production. We also illustrate the potential impact

of our findings on global atmospheric model predictions of several key species, including OH and formic acid, using a 3-D chemistry transport model, CRI-STOCHEM.

Experimental methods

We probed the reaction of CH_2OO with water vapor by complementary time-resolved techniques of broadband cavity-enhanced absorption spectroscopy (TR-BB-CEAS) and synchrotron-based photoionization mass spectrometry (PIMS). Both experiments use heatable flow cells, where reactions are initiated by laser photolysis of appropriate radical precursors. Constant T and P in the reactors are maintained by feedback-controlled resistive heaters and downstream throttle valves; sample composition is regulated by precision flow controllers.

The TR-BB-CEAS apparatus[35,36] is a 1.6 m-long broadband optical cavity that uses continuous "white-light" probe radiation from a Xe arc lamp and operated at probe λ = 300 – 450 nm simultaneously for this study. The cavity is integrated into a quartz laser photolysis flow reactor with ID = 3 cm, capable of operating up to 650 K and 500 Torr. The optical cavity and photolysis laser overlap length is 80 cm. The time evolution of the cavity output spectrum is recorded by a custom spectrometer for each photolysis laser shot and can be averaged indefinitely to obtain sufficient signal-to-noise ratio. For the present work, the wavelength resolution of the spectrometer was 1.5 nm and the temporal resolution was 35 µs. The effective optical path length L_{eff} was measured regularly with known NO_2 concentrations and was typically ~40 – 70 m, depending on the wavelength. Transient absorption spectra were computed from the difference between photolysis laser ON and OFF images:

$$OD(\lambda,t) = -\ln\left(\frac{I_{\text{ON}}(\lambda,t)}{I_{\text{OFF}}(\lambda,t)}\right) = L_{\text{eff}}(\lambda)\sum_i c_i(t)\sigma_i(\lambda) \qquad \text{(E1)}$$

Here I_{ON} and I_{OFF} are the measured probe radiation intensities with/without the photolysis laser; the total transient signal $OD(\lambda,t)$ is the sum of contributions by all absorbing species i with concentrations c_i and absorption cross-sections σ_i.

The multiplexed PIMS apparatus[37] employs a quartz flow reactor with ID = 1.05 cm, capable of T up to 800 K and P up to 50 Torr. A small orifice (300 µm diameter in this study) samples a portion of the gas mixture into a vacuum chamber, where it is skimmed and ionized. The ions are extracted into a pulsed 50 kHz orthogonal acceleration time-of-flight mass spectrometer, which acquires a complete mass spectrum every 20 µs during a time window -20 ms < t < 130 ms, relative to the arrival of the photolysis laser pulse. For the work described here, ionization was performed with tunable, intense (~10^{14} photons·s^{-1}), monochromatic (typical resolution of 20 meV) VUV radiation from the Chemical Dynamics Beamline at the Advanced Light Source, Lawrence Berkeley Lab. The VUV photon energy was scanned over the 9.5 – 11.5 eV range to create a 3-dimensional data set $I(m/z, t, E)$. The PIMS ion signal is described by the formula:[38]

$$I_{m/z}(t,E) = \Lambda \cdot \alpha_{m/z} \cdot \sum_i \big(\sigma_i(E) \cdot c_i(t)\big). \qquad \text{(E2)}$$

The total ion intensity $I_{m/z}(t,E)$ is the sum of signals from all isomers at the mass-to-charge ratio m/z. The quantities $\sigma_i(E)$ and $c_i(t)$ are the energy-dependent photoionization (PI) cross-section and the time-dependent concentration of isomer i; $\alpha_{m/z}$ is the isomer-independent mass discrimination factor, and Λ is the isomer-, mass- and energy-independent sensitivity factor. The

values of Λ and $\alpha_{m/z}$, as well as the experimental mass resolution, were calibrated daily using standard gas mixtures. Time-dependent absolute species concentrations were obtained from raw ion signals using literature absolute photoionization cross-sections, when available, according to a procedure described in detail earlier.[39,40]

Both experiments generated stabilized CH_2OO at room temperature and total pressures 30 – 100 Torr following the scheme developed by Welz *et al*.[6] Chemical reactions were initiated in both flow reactors by photolysis of CH_2I_2 (99% pure) in either He or N_2 bath (both 99.9999%) in the presence of O_2 (99.9999%) and varying amounts of H_2O. CH_2I_2 and distilled H_2O vapor flows were entrained in bath gas flows using temperature- and pressure-controlled glass bubblers. The experimental H_2O concentration was calculated based on the buffer gas flow through the bubbler and the ratio of the H_2O vapor pressure to total bubbler pressure. The validity of this approach was assured by gravimetric measurements of the total amount of water that was removed after long periods of stable flows, with typical errors of less than 2%. Photolysis radiation was provided by a fourth harmonic output of a Nd:YAG laser (266 nm, TR-BB-CEAS experiments) or by an Excimer laser (248 or 351 nm, PIMS experiments). The choice of photolysis wavelength had no effect on the observed kinetics or product distributions.

Results and discussion

Reaction kinetics of CH_2OO with the water monomer and dimer

We initiated the reaction of CH_2OO with water by photolytic production of CH_2I in the presence of O_2 and H_2O in a He or N_2 bath. A summary of all conditions used in the PIMS and UV absorption experiments is given in Table 1. Initial CH_2OO concentrations, estimated using the measured photolysis laser fluence and the UV absorption cross-section of CH_2I_2,[41,42] were sufficiently low, (5 – 9)·10^{11} cm^{-3}, to suppress self-reaction.[43,44] On the other hand, O_2 and H_2O were always in excess, so that the observed kinetics were governed by a simple set of four reactions, R1 – R4:

$$CH_2I_2 + h\nu(266\ nm) \rightarrow CH_2I + I$$
$$CH_2I + O_2 \rightarrow I + CH_2OO \quad (R1)$$
$$CH_2OO + H_2O \rightarrow products \quad (R2)$$
$$CH_2OO + (H_2O)_2 \rightarrow products \quad (R3)$$
$$CH_2OO \rightarrow other\ losses \quad (R4)$$

The reaction R4 above collectively refers to CH_2OO removal by wall loss and by self-reaction. UV absorption is more sensitive to CH_2OO than PIMS; hence, TR-BB-CEAS probing of CH_2OO decays at varying [H_2O] was used to measure the rate coefficients of R2 and R3. To check the validity of describing our chemical system with the simplified mechanism, R1 – R4, we varied O_2 concentration by a factor of ~9.5 and observed no effect on the intensity or decay kinetics of CH_2OO UV absorption. Varying the initial radical concentration by a factor of ~4.2 had no apparent effect on the CH_2OO formation or decay timescales. A detailed mechanism of the $CH_2I + O_2$ reaction system by Lee and Lin[44] indicates that radical-radical reactions other than the CH_2OO self-reaction are not significant under our conditions. Likewise, the products of R2 – R4 are present in such low concentrations (~10^{11} cm^{-3}), that even if their reaction with CH_2OO are

Table 1. Experimental conditions used in PIMS and UV absorption probing of the reaction of CH_2OO with water. All experiments were conducted at T = 293 K.

Set #	Bath gas	P (Torr)	Concentrations, cm^{-3}		
			$[CH_2OO]/10^{11}$ (cm^{-3})	$[O_2]/10^{16}$ (cm^{-3})	$[H_2O]/10^{17}$ (cm^{-3})
MPIMS probing					
1	He	30	5	2.6	0 – 2.7
2	He	30	8.1 – 8.6	6.9 – 7.3	0 – 4.1
3	He	30	8.7 – 9.2	1.3 – 2.6	0 – 2.6
4	He	30	3.6[a]	2.7	2.4
5	He	30	3.2	2.7	2.5[b]
UV absorption probing					
6	He	30	5.2 – 5.5	2.5	0 – 3.3
7	He	50	5.0 – 5.1	2.5	0 – 4.1
8	He	100	4.8 – 5.0	2.5	0 – 3.4
9	He	10 – 50	1.7 – 7.2	0.8 – 7.6	0 – 4.9
10	N_2	50	4.8	2.5	0 – 2.8

[a] – CD_2I_2 was used instead of CH_2I_2 as photolytic precursor to CD_2OO production
[b] – D_2O was used in place of H_2O

very rapid (as in the case of HCOOH[16]) they do not contribute strongly to its removal.
The strong $B^1A' \leftarrow X^1A'$ absorption of CH_2OO has a peak absorption cross-section of ~$1 \cdot 10^{-17}$ cm^2 near 350 nm,[45] providing a straightforward means of direct measurements of its reaction kinetics. In the present study we averaged the transient absorption between 340 and 380 nm, where other spectral signals from IO (a secondary product)[46] or from CH_2I_2 depletion do not contribute significantly. We have previously used the same approach in TR-BB-CEAS probing to investigate the reactivity of CH_2OO with SO_2,[47] formic acid,[16] and isoprene.[48] Figure 1 shows a representative subset of CH_2OO absorption decays at varying $[H_2O]$ along with kinetic fits.

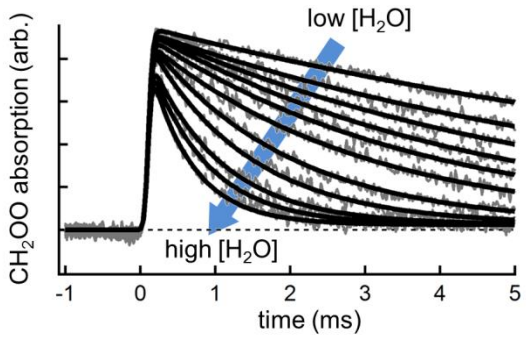

Figure 1. Representative subset of transient UV absorption traces of CH_2OO, taken at T = 293 K and total P = 30 Torr in a He bath, with $[H_2O] = (0 – 3.3) \cdot 10^{17}$ cm^{-3}. The absorption signals (gray lines) were averaged between probe wavelengths λ = 340 and 380 nm. Thick black lines are global fitting results to equation E6 (see text).

Within the simple kinetic framework of reactions R1 – R4, the transient CH_2OO population can be treated as an intermediate species *B* in a reaction sequence:

$$A \xrightarrow{k_1'} B \xrightarrow{k_{decay}'} C \quad \text{(E3)}$$

The rise time of *B* is determined by k_1', the pseudo-first order rate coefficient for the reaction CH_2I + O_2 (R1). The decay rate coefficient k_{decay}' is a sum of three (pseudo-) first order rate coefficients for reactions R2 – R4:

$$k_1' = k_1 \cdot [O_2] \quad \text{(E4)}$$

$$k_{decay}' = k_2' + k_3' + k_4 = k_2 \cdot [H_2O] + k_3 \cdot [(H_2O)_2] + k_4 \quad \text{(E5)}$$

All of the transient UV absorption signals $S(t)$ were fit to a biexponential expression for the time evolution of *B* in the equation E3:

$$S(t) = \frac{A \cdot k_1'}{k_{decay}' - k_1'} \left[e^{-k_1' \cdot t} - e^{-k_{decay}' \cdot t} \right] + S_\infty \quad \text{(E6)}$$

The parameter S_∞ accounts for possible long-time offset due to minor signal contribution from IO or CH_2I_2. All time traces taken at the same pressure and temperature were fit simultaneously. The fit parameter k_1' was fixed in all fits using the known value[49] of k_1 = 1.67·10^{-12} cm^3·s^{-1} and the experimental [O_2]. The fit amplitude *A* and the decay rate coefficient k_{decay}' were allowed to vary, but *A* was treated as a global parameter. The fits were convolved with the experimental time resolution (35µs, independently measured). The rise and decay timescales differed by at least a factor of 10 at all conditions. The results of the fits are shown as black lines in Fig. 1.

A plot of all fitted k_{decay}', corresponding to experimental sets 6 – 10 in Table 1, is presented as a function of [H_2O] in Fig. 2. This plot is strongly curved due to the reaction of CH_2OO with water dimer, whose concentration scales as the square of the monomer concentration. We then fit k_{decay}' vs. [H_2O] to a 2nd-order polynomial, using the literature value of the water dimer equilibrium constant,[50] 0.057 atm^{-1} at *T* = 293 K. The quadratic term yields k_3 = (6.6 ± 0.7)·10^{-12} cm^3·s^{-1}, independent of total pressure, 30 – 100 Torr, or bath gas, He vs. N_2. The errors listed

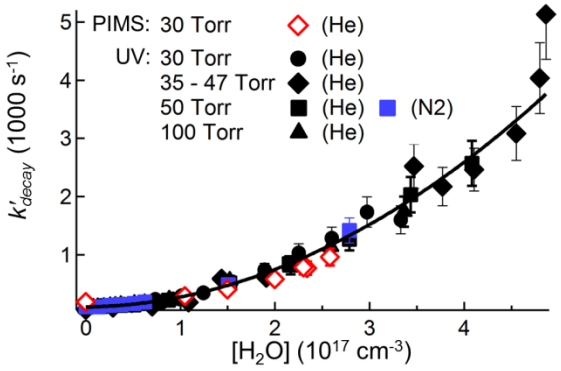

Figure 2. Fitted CH_2OO decay rate coefficients k_{decay}' vs. [H_2O]. The results of all UV absorption and PIMS measurements at P = 30 – 100 Torr in He or N_2 bath gas are shown together. Solid line is a quadratic fit to all UV absorption data simultaneously.

throughout the manuscript are 1σ. The uncertainty in k_2 and k_3 is dominated by the scatter in the measured decays (~10%), but also includes the error in [H_2O] (~2%) and K_{eq} (~3%). Our value is a

near-perfect match to k_3 = 6.5·10^{-12} cm^3·s^{-1} by Chao *et al.*,[19] which was obtained in a similar way to this study: by direct UV absorption probing of CH_2OO, formed *via* reaction R1. However, our result is lower than the value of Berndt *et al.*,[22] k_3 = 1.13·10^{-11} cm^3·s^{-1}, derived from end-product analysis in the ozonolysis of ethene at atmospheric pressure.

The linear term in our fit of k'_{decay} vs. [H_2O] is the rate coefficient k_2 = (2.4 ± 1.6)·10^{-16} cm^3·s^{-1}. Including the linear term in our fit produces noticeable improvement, reducing χ^2 by ~10%, but does not significantly affect k_3 outside its error bounds. The reaction of CH_2OO with the water monomer had been extensively studied before, mostly by relative rate constant measurements that quantified either the removal of reactants by CH_2OO[51] or the end product yields[31,49,52,53] as a function of relative humidity. The values of k_2, derived from those experiments, spanned about 3 orders of magnitude, (2.5 – 3200)·10^{-17} cm^3·s^{-1}. A single study that directly probed CH_2OO decays using PIMS by Welz *et al.*[6] reported an upper limit of k_2 < 4·10^{-15} cm^3·s^{-1}. Calculated values of k_2 similarly vary from 5.8·10^{-18} cm^3·s^{-1} by Ryzhkov *et al.*[17] to 3·10^{-15} cm^3·s^{-1} by Anglada *et al.*[18] Our present measurements fall roughly in the middle of the range of previous results and refine the earlier result of Welz *et al.*[6] Accurate knowledge of k_2 is important to this work because it allows a calculation of the partitioning of the reactive flux among R2 – R4 and hence enables determination of absolute yields, based on PIMS measurements of product concentrations.

Identification of reaction products

PIMS experiments that use tunable VUV ionizing radiation enable the identification of chemical species with isomeric selectivity (e.g. CH_2OO vs. HCOOH) based on their PI spectra. Figure 3 shows a portion of the transient mass spectrum (after subtraction of pre-photolysis signals) with and without H_2O, averaged over time *t* = 0 – 20 ms after photolysis. Under dry conditions, CH_2OO decays mainly by self-reaction and wall losses, and the mass spectrum in the *m/z* = 28 – 66 range contains two intense ion peaks with *m/z* = 30.01 and 46.01, as shown in Fig. 3. Upon the introduction of water, additional peaks appear at *m/z* = 31.02, 47.01, and 64.02. Depletion

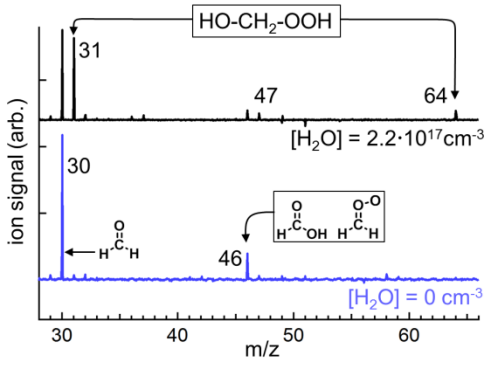

Figure 3. Transient mass spectra with and without H_2O, acquired using ionization energy hν = 11.5 eV and averaged over kinetic times *t* = 0 – 20 ms. Pre-photolysis ion signals have been subtracted.

of CH_2I_2 is visible at the mass of parent ($CH_2I_2^+$, *m/z* = 267.02) and daughter (CH_2I^+, *m/z* = 140.92) ions. Ion peaks due to I, HI, and HOI at *m/z* = 126.90, 127.91, and 143.91, respectively, are also present. The time evolution of these latter peaks indicates slow secondary reactions of the I atom

that do not interfere with the primary chemistry under investigation here; consequently, we omit them from Fig. 3 for clarity.

The minor *m/z* = 47.01 peak has the molecular formula $CH_3O_2^+$. However, its PI spectrum does not match the reference spectrum of methyl peroxy (H_3COO);[54] nor is it due to the hydroperoxymethyl ($HOOCH_2$) radical, which is calculated to be highly unstable.[55-57] The time profile of this peak indicates at least two contributions due to dissociative ionization (DI) of larger compounds, while its lack of dependence on [H_2O] suggests that it does not arise from the reaction R3 (see Figs. S2 and S3). In contrast, the remaining peaks come from the products of R3, as we show below.

The time evolution of all ion peaks relevant to the reaction of CH_2OO with water, obtained at ionization energy of 11.5 eV, is shown in Fig. 4. The *m/z* = 46.01 time trace reveals a strong short-lived and a weaker long-lived component, whereas all other peaks have time profiles characteristic of stable reaction products, rising rapidly to a flat plateau. We assign these peaks to four distinct chemical compounds, based on their measured PI spectra (see Fig. 5), time profiles, exact mass, and mass shift when using deuterated reactants, CD_2I_2 or D_2O, (see Table 1).

The PI spectrum of *m/z* = 30 (CH_2O^+) ions clearly indicates that it is due solely to formaldehyde and enables its quantification, based on the absolute cross-section measurements of Dodson *et al*.[58] The time profile of the *m/z* = 46 ($CH_2O_2^+$) peak suggests two different sources, making its assignment more challenging. The PI spectrum of this peak, averaged over early times, t = 0 – 5 ms, agrees very well with a previously measured spectrum of CH_2OO[6] and contains a minor contribution from HCOOH at energies above 11.3 eV. When averaged over t = 10 – 80 ms, after CH_2OO decays, the PI spectrum of this peak matches that of HCOOH and enables its quantification using the absolute PI cross-section of Cool *et al*.[59] Notably, we find no evidence of dioxirane, which was suggested as a product of R3 in a discharge source.[60] The calculated adiabatic ionization energy (IE_a) of dioxirane is 10.82 eV,[61] yet we detect no *m/z* = 46 ions below 11.3 eV at long delay times and thus conclude that dioxirane is not a significant product of stabilized CH_2OO reactions.

Time-resolved CH_2OO signals in our PIMS experiments have higher noise than the UV absorption time traces, and we could not reliably fit the CH_2OO decays in dataset #1. However, k'_{decay} values obtained from CH_2OO ion signals in datasets #2 and #3 (shown in Fig. S1) agree very well with the UV absorption results and are included in Fig. 2.

We assign the remaining ion peaks at *m/z* = 31 and 64 to the parent cation ($HOCH_2OOH^+$) and dissociative ionization (HO_2 + $HOCH_2^+$) of hydroxymethyl hydroperoxide (HMHP), the main predicted product of R3.[17,18] Calculations at the CBS-QB3 level show a much longer $HOCH_2$–OOH bond in the parent cation (~162 pm) than in neutral HMHP (~141 pm), implying facile dissociation to HO_2 + $HOCH_2^+$. The calculated IE_a of HMHP, averaged over four low-lying rotamers of the neutral compound, is ~9.9 eV; the calculated appearance energy of $HOCH_2^+$ is ~10.7 eV. These values agree with the observed ionization onsets of the *m/z* = 31 and 64 peaks. In experiments using deuterated reactants CD_2OO + H_2O or CH_2OO + D_2O, the ion peaks assigned to HMHP shift to *m/z* = 66 and 33 ($HOCD_2OOH^+$, $HOCD_2^+$) or to m/z = 66 and 32 ($DOCH_2OOD^+$, $DOCH_2^+$). This supports our assignments and confirms the calculated mechanism of HMHP formation by CH_2OO insertion into one of the OH bonds of water.

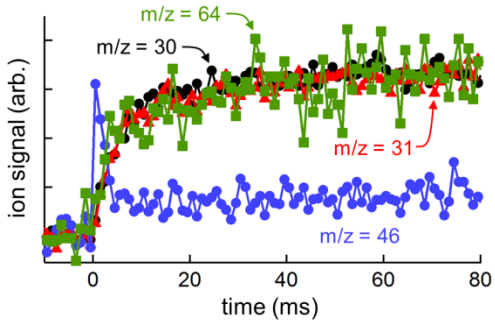

Figure 4. Time evolution of the *m/z* = 30, 31, 46, and 64 ion peaks, obtained with ionization energy $h\nu$ = 11.5 eV at [H_2O] = $2.2 \cdot 10^{17}$ cm^{-3}. All time traces are scaled arbitrarily for visual comparison.

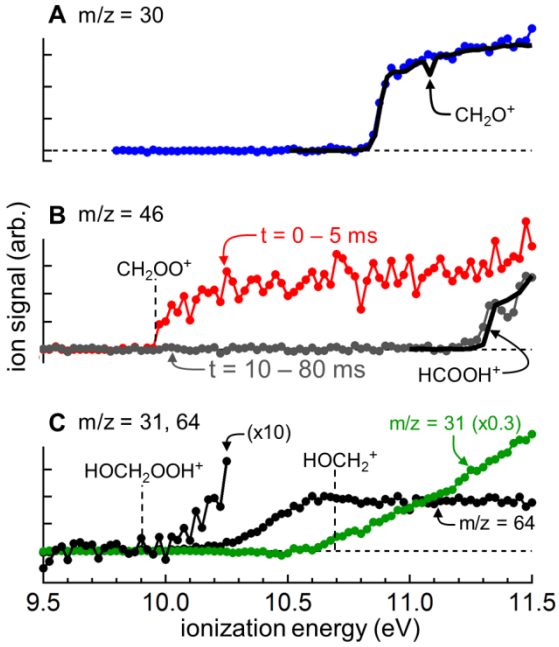

Figure 5. PI spectra of ion peaks, assigned to the products of reactions R1 – R4. *Panel A*: *m/z* = 30 ions, averaged over *t* = 10 – 80 ms (blue dots), along with the literature PI spectrum of CH_2O[58] (black line). *Panel B*: *m/z* = 46 ions, averaged over *t* = 0 – 5 (red) and 10 – 80 ms (gray dots), along with the literature PI spectrum of HCOOH[59] (black line). The dotted line at hν = 10 eV marks the measured ionization energy (IE_a) of CH_2OO.[6] *Panel C: m/z* = 31 and 64, averaged over *t* = 10 – 80 ms. Dotted lines at 9.9 and 10.7 eV show the calculated IE_a of HMHP and the appearance energy of the daughter ion ($HOCH_2^+$), respectively, averaged over four rotational conformers.

Determination of reaction yields

The quantification of formaldehyde and formic acid yields by PIMS allows a determination of reaction yields, provided that the relative importance of all CH_2OO reaction pathways is known. The calculated branching of the total CH_2OO decay into reactions R2 – R4 is shown in Table 2 for experimental sets #1 – 3 (see Table 1). The fractions of the total CH_2OO population that reacts with H_2O, $(H_2O)_2$, or by self-reaction + wall losses (F^{mono}, F^{dimer}, and F^{S+W}) are computed as follows:

$$F^{mono} = k_2'/k_{decay}'$$

$$F^{dimer} = k_3'/k_{decay}'$$

$$F^{S+W} = k_4/k_{decay}'$$

where the definitions of k_2', k_3', k_4, and k_{decay}' are the same as in equation E5. The pseudo-first order rate coefficients k_2' and k_3' were determined using the known concentration of water vapor and the fitted values of k_2 and k_3 from transient UV absorption results. The wall loss, which in large part determines k_4, depends on the reactor size and surface quality; hence, k_4 was directly measured for each of the datasets in Table 2 from the CH_2OO decay under zero-water conditions. The wall loss was relatively rapid in dataset #1, which employed an uncoated quartz reactor, with the observed effective loss rate coefficient k_4 of approximately 480 ± 30 s^{-1}. Subsequent datasets used a reactor coated in halocarbon wax, which significantly reduced wall losses; consequently, k_4 decreased to ~ 180 – 190 s^{-1}.

Table 2 shows that as the water vapor concentration in our PIMS experiments increases from 0 to $4.11 \cdot 10^{17}$ cm^{-3} (equivalent to a partial pressure of ~11.5 Torr or relative humidity of ~66% at room temperature), the fraction of CH_2OO that is lost *via* R4 decreases from 1.0 to 0.07. The value of F^{dimer} correspondingly increases from 0 to 0.9, while the reaction with water monomers remains a minor channel (F^{mono}< 7%) at all conditions. As a result, the CH_2OO removal mechanism shifts from largely by R4 at dry conditions to mostly by R3, reaction with $(H_2O)_2$, at maximum $[H_2O]$. The measured yields of all stable products, averaged over t = 75 – 80 ms in our PIMS experiments, are plotted in Fig. 6 as a function of F^{dimer}. The PI cross-section of HMHP is not known and we therefore plot its relative ion signals in Fig. 6. On the other hand, formaldehyde and formic acid were quantified using known PI cross-sections, which allowed a determination of their branching ratio at $[H_2O]$ = 0 cm^{-3} under the assumption that no other products are formed. PIMS spectra taken at dry conditions with ionization energy 11.5 eV showed no stable products other than CH_2O and HCOOH. Meanwhile, the sum of final concentrations of CH_2O and HCOOH agreed very well with the initial concentration of CH_2OO in the absence of water vapor (see Table 1), supporting our postulate that CH_2O and HCOOH were indeed the only reaction products. From the ratio of CH_2O to HCOOH concentrations at $[H_2O]$ = 0 cm^{-3}, their product branching fractions in the combined CH_2OO wall loss and self-reaction are $\Phi_4(CH_2O)$ = (95 ± 3)% and Φ_4(HCOOH) = (5 ± 3)%. Furthermore, the intensity of CH_2O and HCOOH ion signals at $[H_2O] > 0$, relative to that without water vapor, leads directly to their branching ratio as a function of F^{dimer} as shown in Fig. 6.

All product intensities vary approximately linearly in Fig. 6 and can be extrapolated to F^{dimer} = 1 to determine the branching fractions of R3. The CH_2O absolute yield at F^{dimer} = 1 is computed to be $\Phi_3(CH_2O)$ = (40 ± 10)%. Formic acid yields as a function of F^{dimer} fluctuate between ~2 – 10% of the initial radical concentration, so we settle on a conservative estimate, Φ_3(HCOOH) < 10%. The branching fraction of HMHP is then (55 ± 15)% as long as no other major products of R3 exist – a good assumption, since the other possible product of R3, dioxirane, should be easily detected by PIMS. The listed errors include uncertainties in the signal normalization procedure and in the extrapolation fit. We note that in principle the branching ratios of R2 can also be derived from the above analysis. However, in our experiments

F^{mono} is always small, and the uncertainty in species quantification and in the $(H_2O)_2$ concentration make a determination of product yields of R2 impossible.

Our PIMS experiments also reveal a striking observation. Under dry conditions, the observed rate coefficient of the product rise matches the CH_2OO decay: k'_{decay} ~180 s^{-1}. Yet, although CH_2OO decays progressively faster with increasing water content (k'_{decay} ~2900 s^{-1} at highest $[H_2O]$ used), all products appear with the same rate coefficient of ~220 s^{-1} (see Fig. S4), irrespective of $[H_2O]$. This suggests a long-lived CH_2OO—$(H_2O)_2$ complex, whose decomposition controls product formation. Our results suggest a room-temperature decomposition rate coefficient of ~220 s^{-1} for this complex, which, if confirmed, is a benchmark for calculations of R3 and an important insight into its mechanism.

Table 2. Partitioning of the CH_2OO reactive flux as a function of $[H_2O]$ in PIMS experiments.

Set #	concentrations (cm^{-3})		rate coefficients (s^{-1})			reaction partitioning		
	$[H_2O]/10^{17}$	$[(H_2O)_2]/10^{14}$	k'_2	k'_3	k_4	F^{mono}	F^{dimer}	F^{S+W}
1	2.73±0.14	1.74±0.17	66±44	1150±170	480±30	0.04±0.03	0.68±0.12	0.28±0.03
	0	0	0	0	480±30[a]	0	0	1.0
2	0	0	0	0	190±15[a]	0	0	1.0
	4.1±0.2	3.9±0.4	99±66	2600±380	190±15	0.03±0.02	0.90±0.18	0.07±0.01
	2.20±0.11	1.13±0.11	53±35	740±110	190±15	0.05±0.04	0.75±0.14	0.20±0.03
3	0	0	0	0	178±2[a]	0	0	1.0
	2.58±0.13	1.55±0.16	62±41	1020±150	178±2	0.05±0.03	0.81±0.15	0.14±0.02
	2.34±0.12	1.28±0.13	56±38	840±120	178±2	0.05±0.04	0.78±0.14	0.17±0.02
	2.30±0.12	1.23±0.12	55±37	810±120	178±2	0.05±0.04	0.77±0.15	0.18±0.02
	1.05±0.05	0.26±0.03	25±17	170±25	178±2	0.07±0.05	0.46±0.07	0.47±0.03
	1.50±0.08	0.52±0.05	36±24	350±50	178±2	0.06±0.04	0.62±0.10	0.32±0.03
	2.00±0.10	0.93±0.09	48±32	620±90	178±2	0.06±0.04	0.73±0.13	0.21±0.02

[a] – k_4, obtained at $[H_2O]$ = 0, was applied to all PIMS experiments in the same dataset (i.e. performed on the same day)

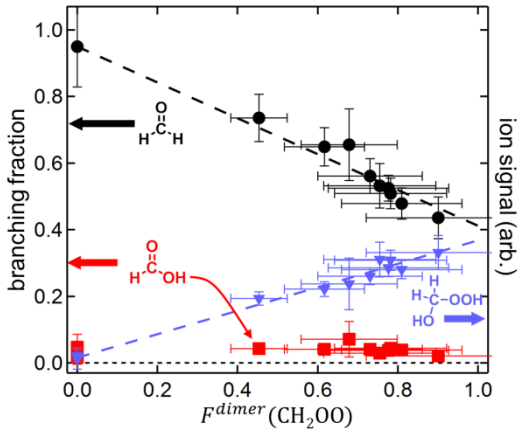

Figure 6. Detected product intensities, averaged over t = 75 – 80 ms, as a function of the CH_2OO fraction reacting with the water dimer, F^{dimer}. The branching fractions of CH_2O and HCOOH (left axis) were determined as described in the text; the relative yields of HMHP (right axis) are the sums of ion counts at m/z = 31 and 64.

The absence of clear experimental signals attributable to such a complex is puzzling. We do not necessarily expect this complex to have an intense UV absorption, especially if its electronic structure differs strongly from bare CH_2OO. However, we cannot easily justify the lack of ion signals arising from this species in our PIMS experiments. It is possible, albeit unlikely, that $CH_2OO–(H_2O)_2$ has vanishingly small ionization cross-sections at the VUV photon energy employed in our study. Another possibility is that at least some of the ion signal at *m/z* = 47 is due to dissociative ionization of $CH_2OO–(H_2O)_2$. Unfortunately, we can't offer a definitive assignment for the *m/z* = 47 ions or a simple explanation for the lack of direct signals from the proposed complex.

Possible influence of wall reactions on measured product yields

Gas sampling in our PIMS experiments occurs at the reactor wall, and the observed reaction kinetics can potentially be affected by heterogeneous processes, e.g. adsorption/ desorption of chemical species or wall reactions. For homogeneous mixtures in a cylindrical geometry, exact analytical solutions can be found for the spatial distributions of the reactants and their time evolution due to wall losses.[62] These solutions depend only on the reactor size and on the characteristic timescales of mass transport in the bulk and at the reactor boundary, as described in detail in the Supporting Material. The decay of reactants near the PIMS reactor wall can therefore be visualized by using their gas-phase diffusion coefficient *D* and wall reaction rate coefficient k_{wall}. Wall effects at the sampling orifice are no more important than elsewhere in the reactor, because the orifice diameter, 300 μm, far exceeds the mean free path in our sample, ~1.7 μm. Although neither *D* nor k_{wall} are known for CH_2OO or the $CH_2OO—(H_2O)_2$ complex, we can estimate their diffusion coefficients by the method of Fuller *et al.*[63] and examine certain limiting cases of k_{wall} to assess the possible effects of wall reactions on our results.

The details of our diffusion modelling are given in figures S5 and S6 and in the accompanying text of the Supporting Material. The upper limits for the diffusion coefficients $D(CH_2OO)$ and $D(CH_2OO—(H_2O)_2)$ are ~14 and 11 cm^2s^{-1} in 30 Torr of pure He. In the presence of H_2O vapor these diffusion coefficients decrease further to $\ll$6 cm^2s^{-1} at the highest $[H_2O]$ employed in this study. The main conclusion that emerges from our analysis is that bulk gas-phase diffusion is far too slow to explain our measured CH_2OO or product time traces. We find that any heterogeneous process with greater than ~100 s^{-1} rate coefficient yields clear non-exponential time evolution of the reactants, with rapid initial decay on the wall, followed by slow, diffusion-limited decay. Such time evolution is inconsistent with our CH_2OO signals in Fig 2, which exhibited unambiguous single-exponential decays up to k'_{decay}~1000 s^{-1}, in excellent agreement with our UV probing results and with literature reports.[19] It is also inconsistent with the 220 s^{-1} exponential rise of reaction products. In effect, diffusion places a lower limit on the apparent reactant decay timescales and on the apparent product rise times, since products cannot form any faster than the reactants decay.

In summary, accurate treatment of possible wall effects on the product yields is challenging and we cannot exclude them completely; however, our analysis suggests that such effects are, at most, minor and that our kinetic model consisting of reactions R1 – R4 adequately captures the overall chemistry. Reaction R4 already accounts for the (relatively minor) CH_2OO wall losses, and no other wall reactions are required. The fact that product yields determined from dataset #1 agree with those from datasets #2 and #3, despite a marked difference in R4, further bolsters this conclusion.

Atmospheric impact

To assess the atmospheric implications of our results, we integrated a global chemistry-transport model CRI-STOCHEM[64] with and without including our measurements of R3, from which we derived the total CH_2OO levels and determined their subsequent effects on tropospheric oxidation cycles. The model combines a reduced chemical mechanism (CRI v2-R5) with a 3-dimensional atmospheric module, driven by archived meteorological data. Extensive descriptions of the original model[65] and subsequent updates,[66-69] including an augmented chemical scheme and an organic aerosol module, are available in the literature. A detailed summary of the model is also included in the Supporting Material. The base case model contains primary emission and oxidation of ethene, propene, trans-2-butene, isoprene, and α-/β-pinene, as well as subsequent CI chemistry. The base case model does not explicitly account for HMHP and assumes rapid conversion of stabilized CI into HCOOH, which therefore represents an upper bound of formic acid production. Conversely, including our measurements of R3 with the assumption that no secondary HCOOH is formed beyond the measured primary yields corresponds to a lower bound of HCOOH production from CI chemistry.

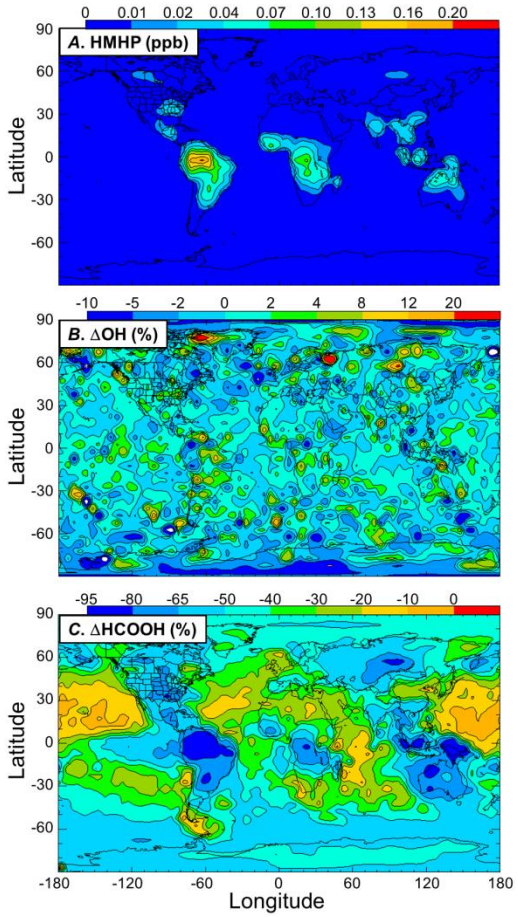

Figure 7. Global impacts of adding the reaction R3 to the CRI-STOCHEM model. *Panel A*: annual average surface mixing ratio of HMHP; *Panel B*: percent change in OH concentrations; *Panel C*: percent change in HCOOH concentrations.

The difference between these two limiting cases of model integration is illustrated in Fig. 7. The global modeled levels of HMHP (Fig. 7A) are in the 10 – 200 ppt range, consistent with field studies.[70,71] Indeed,

because the reaction CH_2OO + water dimer is so rapid, measurements of HMHP might be useful to estimate the tropospheric CH_2OO production rate. The effect of including R3 on the hydroxyl radical concentration is minor, reducing surface OH levels by up to ~5%, largely due to lower production from stabilized CI decomposition. On the other hand, the change in HCOOH levels upon including R3 is a dramatic, decreasing the modeled concentration by 10 – 90 %. The reduction of predicted HCOOH is especially pronounced in equatorial and tropical areas, where comparisons of satellite measurements with models show a significant missing source of HCOOH.[34,72] The model results in Fig. 7 represent an upper bound on the potential atmospheric impact of our measurements, and more studies, especially focusing on the ultimate fate of HMHP, are clearly needed.

Conclusions

We report direct experimental measurements of the reaction kinetics and product branching in the reactions of CH_2OO with water vapor. Transient UV absorption spectroscopy enables accurate determination of the rate coefficients for the reaction $CH_2OO + H_2O$, k_2 =(2.4 ± 1.6)·10^{-16} $cm^3 \cdot s^{-1}$, and $CH_2OO + (H_2O)_2$, k_3 =(6.6 ± 0.7)·10^{-12} $cm^3 \cdot s^{-1}$, at pressures P = 30 – 100 Torr. Our findings resolve the discrepancy in earlier estimates of k_2, which varied by over 3 orders of magnitude. Our value of k_3 is lower than that of Berndt *et al*.[22] using competing kinetics analysis, but matches nearly perfectly the results of Chao *et al*.,[19] obtained by direct UV probing. Concurrent time-resolved tunable VUV PIMS probing provides isomer-selective quantification of the reaction products and allows determination of their absolute yields. We find that at P = 30 Torr and T = 293 K the reaction $CH_2OO + (H_2O)_2$ forms (40 ± 10)% formaldehyde, (55 ± 15)% HMHP, and <10% HCOOH.

The link between CH_2OO reactions and HCOOH is uncertain at this point, and alternative sources of atmospheric HCOOH have also been proposed, including direct emission from vegetation.[73] Contrary to the report of Nguyen *et al*.,[33] our results show that $CH_2OO + (H_2O)_2$ is not a major direct source of HCOOH, producing mainly HMHP and formaldehyde instead. We measure product yields at low pressure; however, increased P usually tends to favor stabilization products (in this case HMHP) so that its yield may be even higher at 1 atm. As Millet *et al*. point out,[34] HMHP itself may ultimately form HCOOH *via* photo-oxidation or heterogeneous conversion. However, the extent of either process in the atmosphere is not known, and further work is clearly needed to clarify its impact.

Acknowledgements

This material is based upon work supported by the Division of Chemical Sciences, Geosciences and Biosciences, Office of Basic Energy Sciences (BES), United States Department of Energy (DOE). DES and MAHK thank the Natural Environment Research Council (NERC) and Bristol ChemLabS for funding various aspects of this work. CJP thanks NERC for funding. This research used resources of the Advanced Light Source, a DOE Office of Science User Facility, which is supported by the Director, Office of Science, BES/DOE, under contract DE-AC02-05CH11231. Sandia National Laboratories is a multi-mission laboratory managed and operated by National Technology and Engineering Solutions of Sandia, LLC., a wholly owned subsidiary of Honeywell International, Inc., for the U.S. Department of Energy's National Nuclear Security Administration under contract DE-NA0003525.

References

1 R. Criegee, *Angew. Chem., Int. Ed. Engl.*, 1975, **14**, 745-752.
2 R. Criegee and G. Wenner, *Liebigs Ann. Chem.*, 1949, **564**, 9-15.
3 D. Johnson and G. Marston, *Chem. Soc. Rev.*, 2008, **37**, 699-716.
4 N. M. Donahue, G. T. Drozd, S. A. Epstein, A. A. Presto and J. H. Kroll, *Phys. Chem. Chem. Phys.*, 2011, **13**, 10848-10857.
5 C. A. Taatjes, D. E. Shallcross and C. J. Percival, *Phys. Chem. Chem. Phys.*, 2014, **16**, 1704-1718.
6 O. Welz, J. D. Savee, D. L. Osborn, S. S. Vasu, C. J. Percival, D. E. Shallcross and C. A. Taatjes, *Science*, 2012, **335**, 204-207.
7 C. A. Taatjes, O. Welz, A. J. Eskola, J. D. Savee, A. M. Scheer, D. E. Shallcross, B. Rotavera, E. P. F. Lee, J. M. Dyke, D. K. W. Mok, D. L. Osborn and C. J. Percival, *Science*, 2013, **340**, 177-180.
8 D. L. Osborn and C. A. Taatjes, *Int. Rev. Phys. Chem.*, 2015, **34**, 309-360.
9 R. Dawes, B. Jiang and H. Guo, *J. Am. Chem. Soc.*, 2015, **137**, 50-53.
10 J. Kalinowski, E. S. Foreman, K. M. Kapnas, C. Murray, M. Räsänen and R. B. Gerber, *Phys. Chem. Chem. Phys.*, 2016, **18**, 10941-10946.
11 R. Harrison, J. Yin, R. Tilling, X. Cai, P. Seakins, J. Hopkins, D. Lansley, A. Lewis, M. Hunter and D. Heard, *Sci. Total Environ.*, 2006, **360**, 5-25.
12 C. J. Percival, O. Welz, A. J. Eskola, J. D. Savee, D. L. Osborn, D. O. Topping, D. Lowe, S. R. Utembe, A. Bacak and G. McFiggans, *Faraday Discuss.*, 2013, **165**, 45-73.
13 K. J. Heaton, R. L. Sleighter, P. G. Hatcher, W. A. Hall IV and M. V. Johnston, *Environ. Sci. Technol.*, 2009, **43**, 7797-7802.
14 J. H. Kroll, J. S. Clarke, N. M. Donahue and J. G. Anderson, *J. Phys. Chem. A*, 2001, **105**, 1554-1560.
15 H.-L. Huang, W. Chao and J. J.-M. Lin, *Proc. Natl. Acad. Sci. U. S. A.*, 2015, **112**, 10857-10862.
16 O. Welz, A. J. Eskola, L. Sheps, B. Rotavera, J. D. Savee, A. M. Scheer, D. L. Osborn, D. Lowe, A. Murray Booth and P. Xiao, *Angew. Chem.*, 2014, **126**, 4635-4638.
17 A. B. Ryzhkov and P. A. Ariya, *Phys. Chem. Chem. Phys.*, 2004, **6**, 5042-5050.
18 J. M. Anglada and A. Solé, *Phys. Chem. Chem. Phys.*, 2016, **18**, 17698-17712.
19 W. Chao, J.-T. Hsieh, C.-H. Chang and J. J.-M. Lin, *Science*, 2015, **347**, 751-754.
20 T. R. Lewis, M. A. Blitz, D. E. Heard and P. W. Seakins, *Phys. Chem. Chem. Phys.*, 2015, **17**, 4859-4863.
21 M. C. Smith, C.-H. Chang, W. Chao, L.-C. Lin, K. Takahashi, K. A. Boering and J. J.-M. Lin, *J. Phys. Chem. Lett.*, 2015, **6**, 2708-2713.
22 T. Berndt, J. Voigtländer, F. Stratmann, H. Junninen, R. L. Mauldin Iii, M. Sipilä, M. Kulmala and H. Herrmann, *Phys. Chem. Chem. Phys.*, 2014, **16**, 19130-19136.
23 S. Gab, E. Hellpointer, W. V. Turner and F. Korte, *Nature*, 1985, **316**, 535-536.
24 A. S. Hasson, G. Orzechowska and S. E. Paulson, *J. Geophys. Res.-Atmos.*, 2001, **106**, 34131-34142.
25 P. Neeb, F. Sauer, O. Horie and G. K. Moortgat, *Atmos. Environ.*, 1997, **31**, 1417-1423.
26 M. Boy, D. Mogensen, S. Smolander, L. Zhou, T. Nieminen, P. Paasonen, C. Plass-Dülmer, M. Sipilä, T. Petäjä and L. Mauldin, *Atmos. Chem. Phys.*, 2013, **13**, 3865-3879.
27 G. Sarwar, K. Fahey, R. Kwok, R. C. Gilliam, S. J. Roselle, R. Mathur, J. Xue, J. Yu and W. P. Carter, *Atmos. Environ.*, 2013, **68**, 186-197.
28 L. Vereecken, H. Harder and A. Novelli, *Phys. Chem. Chem. Phys.*, 2012, **14**, 14682-14695.
29 L. Vereecken, H. Harder and A. Novelli, *Phys. Chem. Chem. Phys.*, 2014, **16**, 4039-4049.
30 J. S. Francisco and W. Eisfeld, *J. Phys. Chem. A*, 2009, **113**, 7593-7600.
31 K. H. Becker, J. Bechara and K. J. Brockmann, *Atmos. Environ., A-Gen.*, 1993, **27**, 57-61.
32 G. E. Orzechowska and S. E. Paulson, *J. Phys. Chem. A*, 2005, **109**, 5358-5365.
33 T. B. Nguyen, G. S. Tyndall, J. D. Crounse, A. P. Teng, K. H. Bates, R. H. Schwantes, M. M. Coggon, L. Zhang, P. Feiner, D. O. Milller, K. M. Skog, J. C. Rivera-Rios, M. Dorris, K. F. Olson, A. Koss, R. J. B. Wild, Stephen S., A. H. Goldstein, J. A. de Gouw, W. H. Brune, F. N. Keutsch, J. H. Seinfeld and P. O. Wennberg, *Phys. Chem. Chem. Phys.*, 2016, **18**, 10241-10254.
34 D. B. Millet, M. Baasandorj, D. K. Farmer, J. A. Thornton, K. Baumann, P. Brophy, S. Chaliyakunnel, J. A. de Gouw, M. Graus, L. Hu, A. Koss, B. H. Lee, F. D. Lopez-Hilfiker, J. A. Neuman, F. Paulot, J. Peischl, I. B. Pollack, B. Ryerson, C. Warneke, B. J. Williams and J. Xu, *Atmos. Chem. Phys.*, 2015, **15**, 6283-6304.
35 L. Sheps and D. W. Chandler, *Time-resolved broadband cavity-enhanced absorption spectrometry for chemical kinetics* SAND2013-2664, Sandia National Laboratories, Livermore, CA, 2013.

36 L. Sheps, A. M. Scully and K. Au, *Phys. Chem. Chem. Phys.*, 2014, **16**, 26701-26706.
37 D. L. Osborn, P. Zou, H. Johnsen, C. C. Hayden, C. A. Taatjes, V. D. Knyazev, S. W. North, D. S. Peterka, M. Ahmed and S. R. Leone, *Rev. Sci. Instrum.*, 2008, **79**, 104103.
38 J. D. Savee, S. Soorkia, O. Welz, T. M. Selby, C. A. Taatjes and D. L. Osborn, *J. Chem. Phys.*, 2012, **136**, 134307.
39 O. Welz, M. P. Burke, I. O. Antonov, C. F. Goldsmith, J. D. Savee, D. L. Osborn, C. A. Taatjes, S. J. Klippenstein and L. Sheps, *J. Phys. Chem. A*, 2015, **119**, 7116-7129.
40 O. Welz, J. Zador, J. D. Savee, L. Sheps, D. L. Osborn and C. A. Taatjes, *J. Phys. Chem. A*, 2013, **117**, 11983-12001.
41 J. C. Mössinger, D. E. Shallcross and R. A. Cox, *J. Chem. Soc., Faraday Trans.*, 1998, **94**, 1391-1396.
42 C. M. Roehl, J. B. Burkholder, G. K. Moortgat, A. Ravishankara and P. J. Crutzen, *J. Geophys. Res.*, 1997, **102**, 12819-12829.
43 Z. J. Buras, R. M. Elsamra and W. H. Green, *J. Phys. Chem. Lett.*, 2014, **5**, 2224-2228.
44 W.-L. Ting, C.-H. Chang, Y.-F. Lee, H. Matsui, Y.-P. Lee and J. J.-M. Lin, *J. Chem. Phys.*, 2014, **141**, 104308.
45 W.-L. Ting, Y.-H. Chen, W. Chao, M. C. Smith and J. J.-M. Lin, *Phys. Chem. Chem. Phys.*, 2014, **16**, 10438-10443.
46 T. J. Gravestock, M. A. Blitz, W. J. Bloss and D. E. Heard, *ChemPhysChem*, 2010, **11**, 3928-3941.
47 L. Sheps, *J. Phys. Chem. Lett.*, 2013, **4**, 4201-4205.
48 Z. Decker, K. Au, L. Vereecken and L. Sheps, *Phys. Chem. Chem. Phys.*, 2017, **19**, 8541-8551.
49 D. Stone, M. Blitz, L. Daubney, N. U. Howes and P. Seakins, *Phys. Chem. Chem. Phys.*, 2014, **16**, 1139-1149.
50 B. Ruscic, *J. Phys. Chem. A*, 2013, **117**, 11940-11953.
51 M. J. Newland, A. R. Rickard, M. S. Alam, L. Vereecken, A. Muñoz, M. Ródenas and W. J. Bloss, *Phys. Chem. Chem. Phys.*, 2015, **17**, 4076-4088.
52 B. Ouyang, M. W. McLeod, R. L. Jones and W. J. Bloss, *Phys. Chem. Chem. Phys.*, 2013, **15**, 17070-17075.
53 M. Suto, E. Manzanares and L. Lee, *Environ. Sci. Technol.*, 1985, **19**.
54 G. Meloni, P. Zou, S. J. Klippenstein, M. Ahmed, S. R. Leone, C. A. Taatjes and D. L. Osborn, *J. Am. Chem. Soc.*, 2006, **128**, 13559-13567.
55 G. L. Vaghjiani and A. Ravishankara, *J. Phys. Chem.*, 1989, **93**, 1948-1959.
56 T. Yamada, J. Bozzelli and T. Lay, *Int. J. Chem. Kinet.*, 2000, **32**, 435-452.
57 L. Vereecken, T. L. Nguyen, I. Hermans and J. Peeters, *Chem. Phys. Lett.*, 2004, **393**, 432-436.
58 L. G. Dodson, L. Shen, J. D. Savee, N. C. Eddingsaas, O. Welz, C. A. Taatjes, D. L. Osborn, S. P. Sander and M. Okumura, *J. Phys. Chem. A*, 2015, **119**, 1279-1291.
59 T. A. Cool, J. Wang, K. Nakajima, C. A. Taatjes and A. Mcllroy, *Int. J. Mass Spectrom.*, 2005, **247**, 18-27.
60 M. Nakajima and Y. Endo, *J. Chem. Phys.*, 2015, **143**, 164307.
61 M. T. Nguyen, T. L. Nguyen, V. T. Ngan and H. M. T. Nguyen, *Chem. Phys. Lett.*, 2007, **448**, 183-188.
62 D. W. Hahn and M. N. Özişik, *Heat Conduction Fundamentals*, 3rd edn., John Wiley & Sons, Hoboken, NJ, USA, 2012.
63 E. N. Fuller, P. D. Schettler and J. C. Giddings, *Industrial & Engineering Chemistry*, 1966, **58**, 18-27.
64 M. E. Jenkin, S. M. Saunders and M. J. Pilling, *Atmos. Environ.*, 1997, **31**, 81-104.
65 W. Collins, D. S. Stevenson, C. Johnson and R. Derwent, *J. Atmos. Chem.*, 1997, **26**, 223-274.
66 R. Derwent, D. Stevenson, R. Doherty, W. Collins, M. Sanderson and C. Johnson, *Climatic Change*, 2008, **88**, 385-401.
67 M. Jenkin, L. Watson, S. Utembe and D. Shallcross, *Atmos. Environ.*, 2008, **42**, 7185-7195.
68 S. Utembe, L. Watson, D. Shallcross and M. Jenkin, *Atmos. Environ.*, 2009, **43**, 1982-1990.
69 L. Watson, D. Shallcross, S. Utembe and M. Jenkin, *Atmos. Environ.*, 2008, **42**, 7196-7204.
70 W. Hua, Z. Chen, C. Jie, Y. Kondo, A. Hofzumahaus, N. Takegawa, C. Chang, K. Lu, Y. Miyazaki and K. Kita, *Atmos. Chem. Phys.*, 2008, **8**, 6755-6773.
71 J. Weinstein-Lloyd, J. Lee, P. Daum, L. Kleinman, L. Nunnermacker and S. Springston, *J. Geophys. Res.*, 1998, **103**, 22361-22373.
72 T. Stavrakou, J. Müller, J. Peeters, A. Razavi, L. Clarisse, C. Clerbaux, P.-F. Coheur, D. Hurtmans, M. De Mazière and C. Vigouroux, *Nat. Geosci.*, 2012, **5**, 26-30.
73 K. Cady-Pereira, S. Chaliyakunnel, M. Shephard, D. Millet, M. Luo and K. Wells, *Atmos. Meas. Tech.*, 2014, **7**, 2297-2311.